Material Modeling and Finite-Element Analysis of Active-contractile and Passive Responses of Smooth Muscle Tissue

A. Grujicic[a],M. Grujicic[b]*, J. S. Snipes[b], R. Galgalikar[b], S. Ramaswami[b]

[a]Department of Bioengineering, [b]Department of Mechanical Engineering
Clemson University, Clemson, SC 29634, USA

*gmica@clemson.edu

Abstract

The present work deals with smooth-muscle-tissue material-model development and its use in finite-element computational analyses. In the first portion of the work, one of the smooth-muscle tissues reported in the open literature is critically assessed. Then, the model is calibrated using experimental data published in the open literature, for isometric (constant length) and isotonic (constant holding stress) uniaxial-tensile-tests of swine carotid artery. Predictions of this model under uniaxial loading conditions are then investigated and their physical soundness is established. Next, the model is implemented into a user-material subroutine which enables, under general deformation conditions, determination of the spatial distribution and temporal evolution of the material stress state and material state-variables. Lastly, the user-material subroutine is linked with a commercial finite-element program and used to analyze a simple smooth-muscle contractile problem involving: (a) a tubular structure surrounded with smooth-muscle tissue (with muscle-cell longitudinal directions aligned in the tube circumferential direction); and (b) an intra-luminal content in the form of a prolate spheroidal, the major axis of which coincides with the tube axis. Activation/contraction of the smooth-muscle tissue triggered by the tube/spheroidal contact stresses has been found to result in a forward momentum/motion of the intra-luminal content.

Keywords

Smooth-muscle Tissue; Contractile Behavior; Finite-element Analysis

Introduction

Within the present work, the contractile response of smooth muscle tissue is analyzed computationally and the response is correlated with the basic architecture/ microstructure of this tissue. Hence, the main aspects of the present work include: (a) basics of smooth muscle tissue; (b) prior computational and experimental work dealing with phenomena and processes accompanying smooth muscle contraction; and (c) multi-scale hierarchical structure of smooth muscle tissue. A brief overview of these aspects of the problem at hand is presented in the remainder of this section.

The Basics of Smooth Muscle Tissue

The defining features of smooth muscle tissue are: (a) unlike skeletal muscle tissue which can undergo only voluntary contractions, smooth muscle tissue undergoes involuntary contractions; (b) its contraction is associated with energy consumption which is ca. 0.2–1% of that associated with skeletal muscle (Brophy, 2000; Paul, 1990; Walker et al., 1994). As a result, smooth muscle tissue is capable of undergoing prolonged contractions without experiencing fatigue (in contrast to skeletal and cardiac muscle) (Morgan et al., 1989); (c) while smooth muscles are capable of delivering comparable isometric (i.e. constant muscle length) force per unit cross-sectional area as skeletal muscle, the rate of smooth muscle contraction is one to two orders of magnitude lower (Bitar, 2003; Walker et al., 1994); (d) smooth muscle tissue is typically found in organs which experience continuing contraction and relaxation such as the stomach, the intestines, the urinary bladder, the airways and blood vessels; and (e) the function of the smooth muscles is generally dependent on the system/organ within which they reside. For example, within the vascular system, blood flow is regulated by the smooth muscle tissue located within the arterial wall. On the other hand, within the digestive system, smooth muscles govern the mixing and transport of intraluminal contents and thus, ensuring: (i) efficient digestion of food; (ii) progressive absorption of nutrients; and (iii) evacuation of residues.

Prior Studies of Smooth Muscle Contraction

The physiology of smooth muscle contraction is highly complex, and involves interaction among a number of (not yet well-understood) electrical, biochemical and

mechanical phenomena and processes. Since abnormalities in smooth muscle contraction can have severe consequences and may cause diseases such as hypertension and asthma, smooth muscle contractions have been the subject of many experimental and theoretical studies.

Among the experimental studies dealing with the smooth-muscle contraction, the following appear the most noteworthy and relevant to the present work: smooth muscle from (a) guinea pig taenia coli (Arner, 1982; Löfgren et al., 2001; Peterson, 1982); (b) porcine carotid artery (Hai and Murphy, 1989; Kamm et al., 1989; Rembold and Murphy, 1988, 1990; Roy et al., 2005; Silver et al., 2003; Singer and Murphy, 1987); (c) porcine coronary artery (Makujina et al., 1995); (d) porcine tracheal (Herrera et al., 2005); (e) canine carotid artery (Takamizawa and Hayashi, 1987); (f) ferret aorta (Jiang and Morgan, 1989); (g) bovine tracheal (Tang et al., 1992); (h) rat aorta (Tosun et al., 1997); and (i) rat pulmonary artery (McIntyre et al., 1996).

As far as the theoretical studies are concerned, they could be broadly divided into two groups: (a) those dealing with the mechanism of smooth muscle contraction (Fay and Delise, 1973; Herrera et al., 2005; Miftakhov and Abdusheva, 1996; Rachev and Hayashi, 1999; Rosenbluth, 1965; Yang et al., 2003a,b); and (b) those focusing on the development of the appropriate continuum-level material constitutive model (Gestrelius and Borgström, 1986; Lee and Schmid-Schönbein, 1996a,b; Stalhand et al., 2008; Zulliger et al., 2004).

The work reported in the present manuscript is most closely related to the work of Kroon (2010) who proposed a theoretical model for the constitutive behavior of smooth muscle tissue, undergoing large deformations. The model includes both the contributions of the calcium-activated contraction and the passive deformation-resistance to the constitutive response of smooth muscle tissue. The active portion of the material response is modeled using the concepts of: (a) contractile units consisting of thick myosin filaments and thin actin filaments; and (b) filament sliding. The passive portion of the material response is of a viscoelastic character and includes the contribution of the remaining intracellular content as well as of the extracellular matrix.

Multi-scale Hierarchical Structure of Smooth Muscle Tissue

As schematically shown in Figure 1(a), smooth muscles possess a layer structure with each layer/sheet containing spindle-shaped cells (each having a single nucleus). Typical dimensions of a smooth muscle cell are: length = 200–300 μm and width = 5–15 μm (Bitar, 2003).

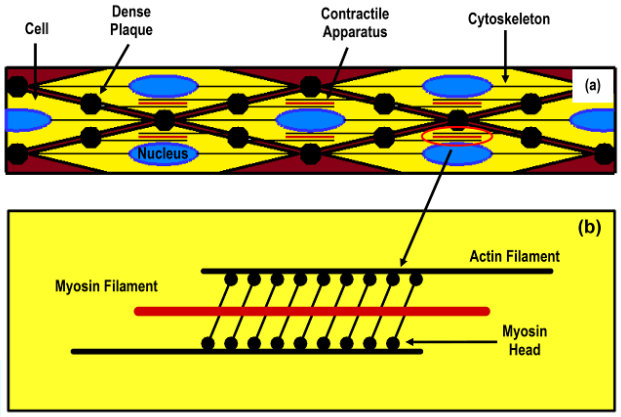

FIGURE 1(a) A SCHEMATIC OF THE SMOOTH-MUSCLE-TISSUE SHOWING LABELED KEY COMPONENTS; AND (b) A SCHEMATIC OF THE CLOSE-UP OF A CONTRACTILE APPARATUS UNIT

Based on their structural/mechanical function, the following main components of a smooth muscle cell are typically identified:

(a) the "contractile apparatus," which consists chiefly of thick myosin filaments and thin actin filaments. It should be noted that in vivo, these filaments are quite labile, and may undergo major structural changes/ reorganizations. Typically, the thin filaments are more abundant, with the ratio of the thin to thick filament numbers as high as 15 in the case of vascular smooth muscle. In general, the myosin/actin contractile-apparatus assemblies are found to be approximately parallel to the cell longitudinal axis (Bitar, 2003; Herrera et al., 2005; Hodgkinson et al., 1995; Kuo and Seow, 2004; Seow and Par, 2007). Often bundles of closely-spaced parallel thick myosin filaments are found to terminate at the same longitudinal location of the cell. Thick filaments in vascular smooth muscles with a typical length of 2.2 μm are longer than their counterparts in skeletal muscle. It should be further noted that to achieve a large contraction stroke and its rate, the length of the contractile unit is quite short in comparison to the cell longitudinal direction (i.e. the number of contractile units across the longitudinal dimension of the cell is quite large).

The architecture of the smooth muscle cells is consistent with the so-called "side-polar conformation" of the thick myosin filaments (the conformation within which cross-bridges on the opposite sides of the filament have opposite orientations), and with the actomyosin side-polar interaction-based filament

sliding model of smooth-muscle contraction (Herrera et al., 2005; Hodgkinson et al., 1995). The sliding filament theory (Huxley, 1953, 1957; Huxley and Niedergerke, 1954; Huxley and Hanson, 1954) postulates that the force required for muscle contraction is produced by advancement of the myosin heads/cross-bridges along the thin actin filaments, Figure 1(b). As seen in Figure 1(b), the side polar model of actomyosin interaction results in the actin filaments that interact with different ends of the thick myosin filament, sliding in opposite directions.

(b) the "cytoskeleton," which contains actin filaments for passive structural support of the cell, as well as intermediate/connecting filaments;

(c) "dense bodies," which contain α-actinin (an actin cross-linking protein) and function as the focal contact points between the contractile apparatus and the cytoskeletal fibers within the cytoplasm. In addition to being a focal point to the actin thin filaments (Hodgkinson et al., 1995), dense bodies are sometimes seen to also act as an anchor to the intermediate filaments. Generally, about 80% of the cell interior is occupied by dense bodies and contractile filaments (Bitar, 2003); and

(d) "dense plaques," the inter-cell focal contact points, located throughout the plasma membrane, which also act as anchors to the actin thin filaments and cytoskeletal intermediate filaments. Since contact interactions between pairs of opposed adjacent dense plaques located on neighboring cells enable force transmission across cell boundaries, the contractile apparatus effectively crosses cell boundaries.

Smooth muscle tissue and their cells are typically analyzed computationally within a continuum framework. That is, structural details of the tissue/cells are smeared out into a homogeneous (often isotropic) continuum. The smooth-muscle-tissue model used and extended in the present work falls into this category of material models. However, there are finer-scale non-continuum material models for the components of the smooth muscle cells. Since, as established above, about 80% of the cell interior is occupied by contractile filaments (including dense bodies) (Bitar, 2003), and these finer-scale material models typically focus on capturing various aspects of constitutive response of the contractile apparatus and its components. As seen in Figure 2, the following additional length-scales/ constitutive models are typically used to capture the behavior of contractile elements and their components: (a) a structural element which models the contracting apparatus as a structural unit consisting of truss-type and beam-type elastic and dissipative elements (Grujicic et al., 2008ab, 2009ab, 2012); (b) a meso-length-scale model within which beads (hypothetical particles composed of a large number of atoms/ions) and coarse-grained molecular statics/dynamics are used to model details of the myosin-head/actin-filament interactions (Chu and Voth, 2005, 2006); and (c) atomic-scale modeling of various aspects of microstructure and properties of different components of the contractile apparatus, e.g. G-actin monomers, F-actin polymers/filaments, etc. (Chu and Voth, 2005; Pfaendtner et al., 2010). As mentioned above, the present work utilizes the concept of a continuum material to treat the contractile and the accompanying passive response of the smooth muscle tissue and cells.

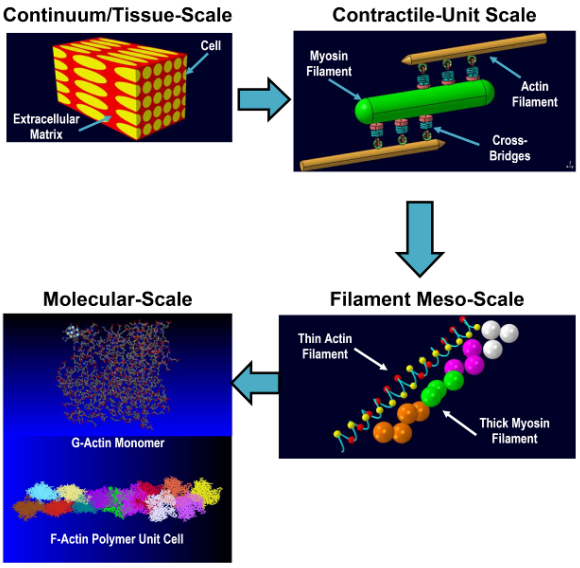

FIGURE 2 MULTI-LENGTH-SCALE HIERARCHICAL STRUCTURE OF THE SMOOTH-MUSCLE-TISSUE

Main Objective

The main objective of the present work is to extend the smooth-muscle-tissue material constitutive model proposed by Kroon (2010) so that the model can be applied within a finite-element computational framework. This extension then enables modeling of the contractile and passive responses of a simple organ, such as a short section of the (small) intestine. As will be shown later, to obtain the extended version of the model proposed by Kroon, a material user subroutine had to be developed and linked with the general-purpose finite element code.

Paper Organization

An overview of the basic biomechanics of smooth muscle contraction is provided in Section II. Chemistry

aspects of the smooth-muscle model proposed by Kroon (2010) are discussed in Section III, while the mechanical aspects of the same model are assessed critically in Section IV. Application of the Kroon model to the cases of isometric (constant muscle length) and isotonic (constant muscle force) uniaxial tensile tests is presented and discussed in Section V. The procedure used to parameterize the model for the case of swine carotid artery smooth-muscle-tissue is described and the resulting model parameters listed in Section VI. Validation of the model as well as an analysis of its key predictions are presented in Section VII. A detailed description of the extension of the material model to the finite-element computational framework and its use to mimic the response of a simplified organ (a short section of the small intestine) is provided in Section VIII. Key conclusions resulting from the present work are summarized in Section IX.

Biomechanics of Smooth Muscle Contraction

Structural and Mechanical Aspects

Since the basic structural and mechanical aspects of smooth-muscle tissue were reviewed in the previous section, they will not be repeated here. Instead, the reader is directed towards reviewing Figures 1(a)–(b) for appropriate details.

Biochemical Aspects

While either mechanical, electrical or chemical stimuli may trigger smooth muscle contraction, in each case muscle contraction is preceded by an increase in the concentration of intracellular Ca^{2+} ions, denoted by $[Ca^{2+}]$ (from ~0.1 μM, corresponding to the relaxed state of the cell, to ~1 μM in the contracted state of the cell).

An increase in the intracellular $[Ca^{2+}]$ sets off the following sequence of biochemical reactions: (i) Ca^{2+} binding to calmodulin is first triggered; (ii) myosin light chain kinase (MLCK) is then activated by the calcium/calmodulin complex which binds to it (Jaggar et al., 2000); and (iii) activation of MLCK in turn activates (independently) each myosin head. Activation of the myosin heads enables cycling/advancement of the cross-bridges (connecting the thick myosin filament to the thin actin filament) along the actin filaments and, in turn, generation of the force required for muscle-cell contraction/ shortening.

The cycling of cross-bridges itself involves a sequence of coupled/correlated biochemical and mechanical phenomena and processes, including: (i) an adenosine triphosphate (ATP) molecule (the source of energy for the contraction) binds to the myosin head, causing its phosphorylation; (ii) the new conformation of the myosin head results in its rapid detachment from actin (if the two were bound); (iii) next, hydrolysis of ATP takes place, which produces adenosine diphosphate and inorganic phosphate (Pi); (iv) a significant change in the myosin-head conformation is associated with the ATP hydrolysis; (v) the myosin-head in the new conformation attaches, through the formation of cross-bridges, to the adjacent actin filament; (vi) next, the Pi dissociates from the myosin head, allowing the release of energy associated with ATP hydrolysis. This, in turn, leads to cycling/peddling of the cross-bridges and to relative sliding between thick myosin filaments and thin actin filaments. To prevent back-sliding of the actin filaments, cross-bridges do not cycle in unison. Examination of the sequence of biochemical and mechanical processes just described reveals that: (a) cell contraction is dependent on the hydrolysis of ATP, the process which provides the necessary chemical energy and its conversion into mechanical work; and (b) the force generated during muscle contraction is a function of the number of cross-bridges connecting the thick myosin filament to, and advancing along, the thin actin filaments (Bitar, 2003).

Under sustained (isometric) contraction conditions, the mechanism of cross-bridge cycling is believed to be different from the one described above. In this case, initial muscle contraction is still activated by an increase in the cytosolic $[Ca^{2+}]$. However, once the maximum contraction of the muscle is attained, the cytosolic $[Ca^{2+}]$ decreases (without an accompanying decrease in contractile stress). In this state, the cross-bridges become dephosphorylated while remaining attached to the actin filaments. This state is commonly referred to as the "latch" state (Dillon et al., 1981) since the cross-bridges either cycle infrequently or do not cycle (Bitar, 2003). In the latch state, cross-bridges remain under tension while maintaining force in sustained muscle contraction. This is accomplished, however, at a level of ATP consumption almost an order of magnitude smaller than the level that would be required under normal cross-bridge cycling conditions (Clark and Pyne-Geithman, 2005).

Chemical Model of Smooth Muscle Contraction

As mentioned earlier, according to the sliding filament theory (Huxley, 1953, 1957; Huxley and Niedergerke, 1954; Huxley and Hanson, 1954), muscle contraction is a result of the relative sliding of myosin and actin filaments within the contractile apparatus. The cross-

bridges play a key role in the biochemistry and mechanics of smooth muscle contraction, as mentioned earlier. The myosin/actin contractile apparatus is simulated in the present work using the model of Hai and Murphy (1988), which postulates the existence of four states (named s_1, s_2, s_3, s_4 respectively) of the cross-bridges. The existence of the four states is a result of the actions of MLCK and myosin light chain phosphatase on both free and actin-attached cross-bridges. According to this model, only phosphorylated cross-bridges are capable of attaching to actin filaments. The four states can be briefly described as follows: (a) when the cross-bridge is in state s_1, it is dephosphorylated and passive and, hence, unable to attach to the actin filament; (b) in state s_2, the myosin head is phosphorylated by the action of the MLCK, i.e. an ATP molecule is attached to the cross-bridge. However, while the myosin head in the s_2 state is capable of attaching to the actin filament, this attachment has not occurred yet; (c) upon attaching to the actin filament, the cross-bridge assumes state s_3. It is the cycling of cross-bridges between states s_2 and s_3 which creates the muscle contractile force; and (d) while remaining attached to the actin filament, some myosin may become dephosphorylated. This (s_4) state of the cross-bridge, as mentioned earlier, is commonly referred to as the latch state. While myosin heads in state 4 do not cycle any further and, hence, do not contribute to relative filament sliding, they generate a passive resistance force within the contractile apparatus (and, thus, help slow down the rate of detachment of the filament heads from the actin filaments). Based on the description of the four myosin-head states, it is clear that only states s_3 and s_4 can generate/transmit force between the myosin and actin filaments.

The contractile-apparatus four-state model of Hai and Murphy (1988) includes the following basic assumptions and simplifications: (a) the total number of myosin heads that may potentially bind to an actin filament, mtot, is assumed to be constant; (b) the fraction of these myosin heads residing, at any instant of time, in state s_i (i=1–4) is denoted as n_i and the four n_i's act as smooth-muscle-contraction chemical-model state variables; (c) evolution of the chemical-model state variables is assumed to be given by a first-order chemical-reaction model in the form

$$\frac{d\mathbf{n}}{dt} = \begin{bmatrix} -k_1 & k_2 & 0 & k_7 \\ k_1 & -k_2 - k_3 & k_4 & 0 \\ 0 & k_3 & -k_4 - k_5 & k_6 \\ 0 & 0 & k_5 & -k_6 - k_7 \end{bmatrix} \mathbf{n} = \mathbf{K}\mathbf{n} \quad (1)$$

where $\mathbf{n} = [n_1\ n_2\ n_3\ n_4]^T$ (the superscript T denotes a transpose operator) is a state-variable column vector while k_1 through k_7 denote rate constants associated with the transitions between different cross-bridge states ($\mathbf{K}$ is the rate-constant matrix); (d) Eq. (1) is subjected to the conservation law which stipulates that the sum of the four n_i's, at any time instant, is equal to 1. It should be noted that, as mentioned earlier, muscle contraction is triggered by an increase in the cytosolic [Ca^{2+}]. Since this increase requires an increase in the value of n_3, it causes an increase in the rate constants k_1 (controlling the s_1– s_2 transition) and k_6 (controlling the s_4– s_3 transition). To help clarify the transition between the four cross-bridge states, a schematic of these states and their inter-relationship is provided in Figure 3.

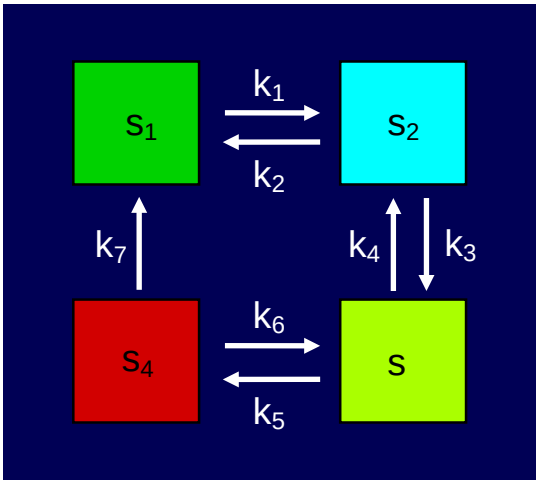

FIGURE 3 FOUR STATES OF THE CROSS-BRIDGES PROPOSED BY HAI AND MURPHY (1988), AND LABELS FOR THE RATE CONSTANTS RELATED TO THE TRANSITIONS BETWEEN DIFFERENT STATES

Mechanical Model of Smooth Muscle Contraction

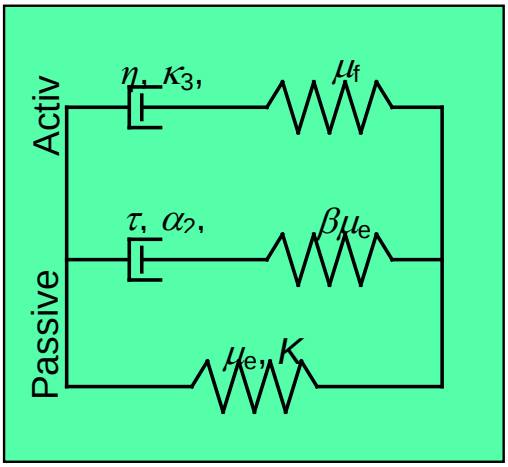

FIGURE 4 RHEOLOGICAL MODEL OF THE SMOOTH-MUSCLE TISSUES PROPOSED BY KROON (2010). PLEASE SEE TEXT FOR DETAILS

According to the preceding discussion and Figure 1(a), contractile-apparatus filaments are approximately aligned in the cell longitudinal direction and transcend the cell boundaries. In the lateral direction, these filaments are closely-spaced and parallel, with the myosin heads located at fairly regular longitudinal intervals. Taking this consideration into account, Kroon (2010) proposed a muscle-cell mechanical model which contains the following elements/ assumptions: (a) contractile-apparatus filaments are assumed to all be parallel, aligned with the cell longitudinal direction and surrounded by a passive matrix. The latter contains: (i) the remainder of the cell interior (composed of cell membrane, cytosol, passive networks of actin, intermediate filaments, cell nuclei); and (ii) extracellular matter typically composed of elastin and collagen; (b) to capture this behavior, the corresponding rheological model is constructed which contains three parallel branches, one "*active*" (generates the contractile force) and two passive (Figure 4), aligned in the muscle-cell longitudinal direction; (c) the constitutive response of the rheological model displayed in Figure 4 is described using the large-deformation formalism and the concept of the strain-energy (density) function Ψ as:

$$\Psi = \Psi_{\text{act}} + \Psi_{\text{pass}} \tag{2}$$

where subscripts *act* and *pass* are used to denote the active and passive components of Ψ; (d) to account for the potentially large deformation and rotations accompanying muscle contraction, a single Cartesian coordinate system defined in terms of three basis vectors $\mathbf{e}_1, \mathbf{e}_2, \mathbf{e}_3$ is first introduced. Then, the position vectors of a material point in the reference configuration Ω_0 and the current configuration Ω are defined as $\mathbf{X} = X_i \mathbf{e}_i$ and $\mathbf{x} = x_i \mathbf{e}_i$, respectively; (e) the kinematics of deformation is next described using the deformation gradient $\mathbf{F}$:

$$\mathbf{F} = \partial \mathbf{x} / \partial \mathbf{X}, \tag{3}$$

right Cauchy-Green deformation tensor, $\mathbf{C}$:

$$\mathbf{C} = \mathbf{F}^T \mathbf{F} \tag{4}$$

and the Green-Lagrange strain $\mathbf{E}$:

$$\mathbf{E} = \frac{\mathbf{1}}{\mathbf{2}}(\mathbf{C} - \mathbf{I}) \tag{5}$$

where $\mathbf{I}$ is the second-order identity tensor; (f) the stress state is defined by the second Piola-Kirchhoff stress $\mathbf{S}$ as:

$$\mathbf{S} = \frac{\partial \psi}{\partial \mathbf{E}} = 2\frac{\partial \psi}{\partial \mathbf{C}} = 2\frac{\partial \psi_{\text{act}}}{\partial \mathbf{C}} + 2\frac{\partial \psi_{\text{pass}}}{\partial \mathbf{C}} = \mathbf{S}_{\text{act}} + \mathbf{S}_{\text{pass}}, \tag{6}$$

by the first Piola-Kirchhoff stress $\mathbf{P}$ as:

$$\mathbf{P} = \mathbf{FS} = \mathbf{F}\left(\mathbf{S}_{\text{act}} + \mathbf{S}_{\text{pass}}\right) = \mathbf{P}_{\text{act}} + \mathbf{P}_{\text{pass}}, \tag{7}$$

and by the Cauchy (true) stress $\boldsymbol{\sigma}$ as:

$$\boldsymbol{\sigma} = \mathbf{FSF}^T / \det \mathbf{F} \tag{8}$$

where *det* denotes a determinant operator.

Active Part of the Mechanical Response

As shown in Figure 4, the contractile apparatus is modeled using one of the three branches, i.e. the active branch. The main characteristics of the active branch can be summarized as follows: (a) this branch is assumed to consist of an "*active dashpot*" (a contractile-force-generating time-dependent element) and a passive spring. The active dashpot is used to describe the cycling behavior of the cross-bridges which results in relative filament sliding, while the passive spring is used to describe the elastic resistive response of the cross-bridges. It should be noted that the myosin thick filaments and actin thin filaments, in the present contractile-apparatus formulation, are treated as rigid bodies. In other words, the entire filament-sliding and passive-resistance response of the contractile element is assumed to be localized within the myosin heads; (b) the active branch is aligned with direction $\mathbf{M}$ (defined as a unit column vector) in the reference configuration Ω_0; (c) stretching of the (entire) structural element in the filament direction (i.e. direction $\mathbf{M}$), λ_f, is defined as $\lambda_f^2 = \mathbf{M}^T \mathbf{C} \mathbf{M}$. The effect of filament contraction is depicted in Figure 5, which shows that the distance between two adjacent dense bodies (bridged by a contractile-apparatus) has been reduced from its initial value L_{cu} (in the reference configuration) to $\lambda_f L_{cu}$ (in the current configuration); (d) within the active branch, λ_f is decomposed multiplicatively as $\lambda_f = \lambda_e \lambda_{fc}$, where λ_{fc} accounts for the relative sliding between myosin and actin filaments (*fc* stands for filament contraction) and λ_e accounts for the elastic deformation of the cross-bridges; (e) the following "*active strain energy function*" is utilized (Fung, 1970):

$$\begin{aligned} \psi_{\text{act}} &= \frac{\mu_f}{4}(n_3 + n_4)\left(\lambda_e^2 - 1\right)^2 \\ &= \frac{\mu_f}{4}(n_3 + n_4)\left(\frac{\mathbf{MCM}}{\lambda_{fc}^2} - 1\right)^2 \end{aligned} \tag{9}$$

where: (i) μ_f is a stiffness parameter which is proportional to the stiffness of cross-bridges and to the number of parallel contractile filaments per unit area of the cell transverse section; (ii) the fact that only cross-bridges in states s_3 and s_4 contribute to a force generation/transmittal within the active branch is

reflected by the use of the $(n_3 + n_4)$ term; (iii) cross-bridges in states s_3 and s_4 are assumed to possess the same elastic stiffness; (iv) the total number of myosin heads, at a given level of [Ca^{2+}], participating in the construction of a contractile apparatus, m_{tot}, remains constant; and (v) the functional form of ψ_{act} ensures that, in the relaxed state, not only the strain energy but also the three aforementioned stress measures are zero; and (f) examination of the active-branch mechanical model shows that it is associated with four state variables (i.e. variables which define the current state of the contractile-apparatus): n_3, n_4, λ_f and λ_{fc}. To compute the instantaneous values of these state variables, the corresponding evolution equations must be defined and integrated in time.

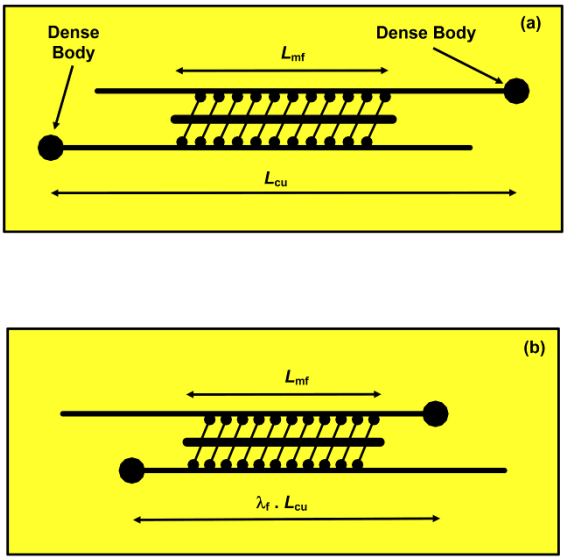

FIGURE 5 A SCHEMATIC OF THE FILAMENT SLIDING MECHANISM FOR SMOOTH MUSCLE CONTRACTION SHOWING: (A) THE RELAXED; AND (B) THE CONTRACTED CONFIGURATIONS OF A SINGLE CONTRACTILE-APPARATUS

1) Evolution Equations for n_3 and n_4

Evolution of n_3 and n_4 has been previously defined using Eq. (1).

2) Evolution Equation for λ_f

Since $\lambda_f^2 = \mathbf{M}^T\mathbf{C}\mathbf{M}$, its evolution is defined by the temporal evolution of $\mathbf{C}$ (i.e. of $\mathbf{F}$).

3) Evolution Equation for λ_{fc}

Kroon (2010) proposed the following evolution equation for λ_{fc}:

$$\eta\dot{\lambda}_{fc} = P_{cc} - \frac{\partial\psi_{act}}{\partial\lambda_{fc}} \tag{10}$$

where P_{cc} denotes the active stress generated by the active dashpot in response to an increase in [Ca^{2+}], η is a viscous-damping coefficient associated with the cross-bridge-cycling/fiber-contraction process, and the term $-\partial\psi_{act}/\partial\lambda_{fc}$ is the elasticity-type myosin-head resistance to fiber contraction. To construct the appropriate expression(s) for P_{cc}, Kroon made the following observations: (a) since P_{cc} is generated as a result of muscle-cell contraction, this term is of a compressive-negative character; (b) only phosphorylated and attached cross-bridges in state s_3 contribute to filament contraction; (c) when P_{cc} does not possess a sufficiently high magnitude to cause further muscle contraction, but is comparable to $\partial\psi_{act}/\partial\lambda_{fc}$, dephosphorylated attached cross-bridges in state s_4 can help prevent backsliding in the contractile filaments; (d) when the elastic-resistance term $-\partial\psi_{act}/\partial\lambda_{fc}$ exceeds the magnitude of P_{cc}, the dephosphorylated cross-bridges become detached from the actin filaments and no longer contribute to the load transfer within the active branch. While cross-bridges in state s_3 may also get detached, their phosphorylated character allows them to quickly reattach to the contracting filament and to slow down the rate of filament backsliding/extension. To capture this behavior of the active branch, Kroon proposed the following expressions for P_{cc}: (i) for the contracting state of the filament ($\dot{\lambda}_{fc} < 0$), within which the magnitude of the active stress exceeds the elastic resistance:

$$P_{cc} = -\kappa_3 n_3, \quad \text{for } \kappa_3 n_3 \geq -\frac{\partial\psi_{act}}{\partial\lambda_{fc}} \tag{11}$$

(ii) for the intermediate state of the filament ($\dot{\lambda}_{fc} = 0$), which is characterized by nearly zero changes in λ_{fc}:

$$P_{cc} = \frac{\partial\psi_{act}}{\partial\lambda_{fc}}, \quad \text{for } \kappa_3 n_3 < -\frac{\partial\psi_{act}}{\partial\lambda_{fc}} \leq \kappa_3 n_3 + \kappa_4 n_4 \tag{12}$$

(iii) for the backsliding/extension state of the filament ($\dot{\lambda}_{fc} > 0$):

$$P_{cc} = -\kappa_3 n_3, \quad \text{for } \kappa_3 n_3 + \kappa_4 n_4 < -\frac{\partial\psi_{act}}{\partial\lambda_{fc}} \tag{13}$$

where κ_3 and κ_4 reflect the intensity/strength of the filament-contraction driving force and the filament-contraction elastic resistance, respectively.

Specification of ψ_{act} via Eq. (9) and the functional

relationship given in Eq. (6) enables determination of the active second Piola-Kirchhoff stress as:

$$\mathbf{S}_{\text{act}} = 2\frac{\partial \psi_{\text{act}}}{\partial \mathbf{C}} = \frac{\mu_{\text{f}}\left(\text{n}_3 + \text{n}_4\right)}{\lambda_{\text{fc}}^2}\left(\frac{\mathbf{M}^{\text{T}}\mathbf{C}\mathbf{M}}{\lambda_{\text{fc}}^2} - 1\right)\mathbf{M}\otimes\mathbf{M} \quad (14)$$

where $\otimes$ denotes the dyadic product of two vectors.

4) Summary of the Model Parameters

Examination of Eq. (14) shows that the active part of the smooth-muscle-tissue mechanical model contains four material parameters: μ_f, κ_3, κ_4 and η.

Passive Part of the Mechanical Response

1) Decomposition of the Deformation Gradient

The passive part of the smooth-muscle material is treated as being isotropic linear-viscoelastic and is modeled using a generalized Maxwell model consisting of two parallel branches, Figure 4. In addition, in accordance with the general practice, it is assumed that only the isochoric (i.e. volume-conserving) part of deformation can be viscous (i.e. time-dependent). In other words, the volumetric part of deformation is assumed to be purely elastic. Consequently, the total deformation gradient is decomposed multiplicatively as:

$$\mathbf{F} = J^{1/3}\hat{\mathbf{F}} \quad (15)$$

where $J = \det\mathbf{F}$ is a measure of the deformation-induced volume change, and $\hat{\mathbf{F}}$ defines the isochoric part of the deformation gradient (i.e. $\det\hat{\mathbf{F}} = 1$).

Since stresses arise solely from the elastic part of the deformation, the isochoric part of the deformation must be further decomposed into its viscous and elastic parts as:

$$\hat{\mathbf{F}} = \hat{\mathbf{F}}_e\mathbf{F}_v \quad (16)$$

where subscripts e and v are used to denote, respectively, the elastic and the viscous parts of a quantity, and both $\hat{\mathbf{F}}_e$ and $\mathbf{F}_v$ are isochoric.

Using the relation given by Eq. (4), the total isochoric, elastic and viscous types of the right Cauchy-Green deformation tensors can be defined as:

$$\hat{\mathbf{C}} = \hat{\mathbf{F}}^T\hat{\mathbf{F}} \quad (17)$$

$$\hat{\mathbf{C}}_e = \hat{\mathbf{F}}_e{}^T\hat{\mathbf{F}}_e \quad (18)$$

$$\mathbf{C}_v = \mathbf{F}_v{}^T\mathbf{F}_v \quad (19)$$

2) Passive-Strain-Energy Function

The passive part of the strain-energy function is defined as the sum of three (i.e. volumetric, elastic-isochoric and viscous) terms as:

$$\begin{aligned}\psi_{\text{pass}} &= \psi_{\text{pass}}(J, \hat{\mathbf{C}}, \mathbf{C}_{\text{v}}) \\ &= U(J) + \psi_{\infty}(\hat{\mathbf{C}}) + \psi_{v}(\hat{\mathbf{C}}, \mathbf{C}_{\text{v}})\end{aligned} \quad (20)$$

where the three parts (U, ψ_∞, ψ_v) of the passive-strain-energy function are, respectively, defined as:

$$U(J) = \frac{1}{2}K(J-1)^2 \quad (21)$$

$$\psi_{\infty} = \frac{\mu_e}{2}\left(\text{tr}\hat{\mathbf{C}} - 3\right) = \frac{\mu_e}{2}\left(I_3^{-1/3}\mathbf{C} : \mathbf{I} - \mathbf{3}\right) \quad (22)$$

$$\psi_{v} = \frac{\beta\mu_e}{2}\left(\hat{\mathbf{C}}_e : \mathbf{I} - \mathbf{3}\right) = \frac{\beta\mu_e}{2}\left(I_3^{-1/3}\mathbf{C} : \mathbf{C}_v^{-1} - \mathbf{3}\right) \quad (23)$$

where K, the bulk modulus, and μ_e, the steady-state "*shear-spring constant*" of the passive part of the muscle, are associated with the bottom (single-spring branch) in Figure 4, and $I_3 = J^2$ is the third invariant of $\mathbf{C}$. $\beta\mu_e$ denotes the shear-spring constant within the second/viscous branch while $:$ represents the inner/scalar product of two second-order tensors.

Examination of Eqs. (21)–(23) reveals that the deformation state of the passive part of the smooth-muscle-tissue mechanical model is defined by $\mathbf{C}$ and $\mathbf{C}_v$ (and their invariants).

3) Passive-Stress Components

Via the use of Eqs. (6) and (21)–(23), the corresponding components of the passive second Piola-Kirchhoff stress can be derived as:

$$\mathbf{S}_{\text{vol}} = K(J-1)J\mathbf{C}^{-1} \quad (24)$$

$$\mathbf{S}_{\infty} = \mu_e I_3^{-1/3}\left(\mathbf{I} - \frac{1}{3}(\mathbf{C} : \mathbf{I})\mathbf{C}^{-1}\right) \quad (25)$$

$$\mathbf{S}_{v} = \beta\mu_e I_3^{-1/3}\left(\mathbf{C}_v^{-1} - \frac{1}{3}(\mathbf{C} : \mathbf{C}_v^{-1})\mathbf{C}^{-1}\right) \quad (26)$$

while the total passive second Piola-Kirchhoff stress is given as:

$$\begin{aligned}\mathbf{S}_{\text{pass}} &= 2\frac{\partial \psi_{\text{pass}}}{\partial \mathbf{C}} \\ &= 2\frac{\partial U(J)}{\partial \mathbf{C}} + 2\frac{\partial \psi_{\infty}}{\partial \mathbf{C}} + 2\frac{\partial \psi_{\text{v}}}{\partial \mathbf{C}} \\ &= \mathbf{S}_{\text{vol}} + \mathbf{S}_{\infty} + \mathbf{S}_{v}\end{aligned} \quad (27)$$

The corresponding expressions for the first Piola-Kirchhoff stress and for the Cauchy stress can be obtained using Eqs. (7)–(8), respectively.

4) Evolution Equation for $\mathbf{S}_v$:

Examination of Eq. (23) shows that as $\mathbf{C}_v$ relaxes towards $\hat{\mathbf{C}} = I_3^{-1/3}\mathbf{C}$, ψ_v, and hence, $\mathbf{S}_v$ vanish. In

order to capture time evolution of the viscous second Piola-Kirchhoff stress and to obtain a reasonable agreement with the experimental data, Kroon (2010) proposed the following functional relationship:

$$\left(\left.\frac{d\mathbf{S}_v}{dt}\right|_{\mathbf{C}=\text{const}}\right)_{ij} = \left(\frac{\partial \mathbf{S}_v}{\partial \mathbf{C}_v} : \dot{\mathbf{C}}_v\right)_{ij} = -\frac{1}{\tau}\left(S_{v,ij} + \alpha_2 \text{sgn}(S_{v,ij}) S_{v,ij}^2 + \alpha_3 S_{v,ij}^3\right) \quad (28)$$

where τ is the relaxation time. Typically, only the first term associated with the exponential relaxation of the form $\exp(-t/\tau)$, where t is time, is used. However, in order to obtain a good agreement with the experimental results, Kroon found it necessary to introduce the two additional non-linear terms in Eq. (28) with α_2 and α_3 being the corresponding coefficients. It should be noted Eq. (28) implicitly defines $\dot{\mathbf{C}}_v$ and, hence, the evolution of $\mathbf{C}_v$.

5) Summary of the Model Parameters

Examination of Eqs. (15)–(28) shows that the passive part of the smooth-muscle model includes the following model parameters: K, μ_e, β, τ, α_2 and α_3.

Thermodynamic Validity of the Model

Kroon (2010) also established that the model is thermodynamically valid, i.e. the internal energy is always non-negative, provided the following two conditions are satisfied: (a) $\eta \geq 0$; and (b) $\left(-\partial\psi/\partial C_v\right) : \dot{C}_v \geq 0$.

Model Reduction for Uniaxial Tensile Loading Case

Since the muscle-cell material-model parameters, summarized in the previous sections, are typically determined using laboratory uniaxial tensile tests, it is beneficial to recast the model into its uniaxial tensile form. This is done in the present section. It should be noted that, for convenience, the filaments are aligned in the $\mathbf{e_3}$ direction, i.e. $\mathbf{M} = \mathbf{e_3}$.

1) Deformation Variables

(a) Deformation gradient– $\mathbf{F} = diag(\lambda_1, \lambda_2, \lambda_3)$ where *diag* denotes a diagonal second-order tensor, and λ_i's$(i = 1-3)$ are the three principal stretches; (b) Viscous deformation gradient–$\mathbf{F}_v = diag(\lambda_{v,1}, \lambda_{v,2}, \lambda_{v,3})$; (c) Due to symmetry/transverse-isotropy, $\lambda_1 = \lambda_2$ and $\lambda_{v,1} = \lambda_{v,2}$; (d) Due to the isochoric character of $\mathbf{F}_v$, $\lambda_{v,1}\lambda_{v,2}\lambda_{v,3} = 1$ or $\lambda_{v,1} = \lambda_{v,2} = 1/\sqrt{\lambda_{v,3}} = 1/\sqrt{\lambda_v}$; (e) $\mathbf{C} = diag(\lambda_1^2, \lambda_1^2, \lambda_3^2)$; (f) $\lambda_f^2 = \mathbf{e_3}^T \mathbf{C} \mathbf{e_3} = \lambda_3^2$, $\lambda_f = \lambda_3$ and $\lambda_e = \lambda_3 / \lambda_{fc}$. Thus, within the uniaxial stress framework, the deformation state of the smooth-muscle material is defined by the following four scalar parameters: λ_1, λ_3, λ_v and λ_{fc}.

2) Stress State

In the case of the uniaxial tensile test in the $\mathbf{e_3}$ direction, only the (3,3)-component of different stress measures are nonzero. Specifically, the (3,3)-component of the first Piola-Kirchhoff stress is defined as:

$$\begin{aligned} P_{33} = {} & \mu_f\left(n_3 + n_4\right)\left(\frac{\lambda_3^3}{\lambda_{fc}^4} - \frac{\lambda_3}{\lambda_{fc}^2}\right) + K\left(J-1\right)\lambda_1^2 \\ & + \frac{\mu_e I_3^{-1/3}}{3}\left(3\lambda_3 - \frac{I_1}{\lambda_3}\right) + \frac{2\beta\mu_e I_3^{-1/3}}{3}\left(\frac{\lambda_3}{\lambda_v^2} - \frac{\lambda_1^2\lambda_v}{\lambda_3}\right) \end{aligned} \quad (29)$$

where the four terms on the right-hand side of Eq. (29) denote respectively the active, the volumetric, the steady-state and the viscous stress components, $I_1 = 2\lambda_1^2 + \lambda_3^2$ denotes the first invariant (i.e. the trace) of $\mathbf{C}$. The lateral first Piola-Kirchhoff stresses $P_{11} = P_{22}$ are zero and are defined by the following functional relationship:

$$\begin{aligned} P_{11} = {} & P_{22} \\ = {} & K(J-1)\lambda_1\lambda_3 + \frac{\mu_e I_3^{-1/3}}{3}\left(3\lambda_1 - \frac{I_1}{\lambda_1}\right) \\ & + \frac{\beta\mu_e I_3^{-1/3}}{3}\left(\lambda_1\lambda_v - \frac{\lambda_3^2}{\lambda_1\lambda_v^2}\right) \\ = {} & 0 \end{aligned} \quad (30)$$

Eq. (30) provides a functional relationship between λ_3 and λ_1 (i.e. λ_1 is not an independent deformation variable, but rather a variable whose value is constrained through the zero-lateral-stress condition, Eq. (30)). The corresponding second Piola-Kirchhoff stress and Cauchy stress can be obtained by combining Eq. (7) with Eqs. (6) and (8).

3) Evolution Equations

To complete the uniaxial-stress formulation of the smooth-muscle-tissue material model, previously defined evolution equations must be used either in their original form or after reformulation. Specifically: (a) Eq. (1) must be used (in the original form) to track the evolution of n_3 and n_4; (b) Eq. (6) must be used (in the original form) to determine

temporal evolution of λ_{fc}; and (c) Eq. (28) must be used to compute temporal evolution of $S_{v,33}$, and in turn $P_{v,33}$ and $\sigma_{v,33}$.

4) Integration of the Material State:

To determine the evolution of the material state during uniaxial tensile loading, the algebraic and differential evolution equations must be combined and solved incrementally in time. Loading could be either stress-controlled (in which case one would determine the temporal evolution of λ_3, as well as the evolution of the remaining deformation and state variables), or stretch-controlled (in which case one would compute the temporal evolution of the longitudinal stress, as well as the evolution of the remaining deformation and state variables).

Parameterization of the Model

To parameterize the model overviewed in the previous section, Kroon (2010) used isometric (constant specimen-length) and isotonic (constant total longitudinal stress) uniaxial-tensile-test data for swine-carotid-artery smooth-muscle tissue as reported in the work of Dillon et al. (1981) and Dillon and Murphy (1982).

Parameterization of the Chemical-state Rate Constants

In Section III, it was shown that the chemical part of the model is defined in terms of seven rate constants, k_1–k_7. To determine these constants, Kroon utilized the following approach: (a) since rate constants k_3, k_4 and k_7 are found to be fairly similar for different types of smooth muscle, typical values reported in the open literature ($k_3 = 4k_4$, $k_4 = 0.11$ s^{-1}, $k_7 = 0.01$ s^{-1}) are adopted; (b) for rate constants k_2 and k_5, the values ($k_2 = 0.5$ s^{-1}, $k_5 = 0.5$ s^{-1}) obtained by Hai and Murphy (1988) for swine-carotid-artery smooth-muscle are used; (c) as far as the remaining rate constants, i.e. k_1 and k_6 are concerned, it was first recognized that since they indirectly or directly affect the (isometric steady-state) fraction of cross-bridges in states s_3 and s_4 and thus the magnitude of the active stress, these rate constants are functions of cytosolic [Ca^{2+}]. As [Ca^{2+}] increases, k_1 and k_6 start to dominate the remaining rate constants and ultimately, at very high values of [Ca^{2+}] solely control and result in the maximum isometric steady-state value of ($n_3 + n_4$). k_1 and k_6, at a given level of [Ca^{2+}], are then obtained by taking advantage of the fact that the ratio of the corresponding active stress and that at the maximum activation level, is equal to the corresponding ratio of the ($n_3 + n_4$) sum. This procedure yielded $k_1 = k_6 = 0.14$ s^{-1} for [Ca^{2+}] = 1.6 mM (Dillon and Murphy, 1982).

It should be noted that the values of k_1 and k_6 are affected by the cytosolic [Ca^{2+}]. The values for these two rate constants reported above correspond to the cytosolic [Ca^{2+}] of 1.6 mM, the concentration, which was maintained constant during the isometric and isotonic tensile tests (described in the remainder of this section).

Parameterization of the active part of the model

As mentioned earlier, the active part of the mechanical model is characterized by four parameters: μ_f, κ_3, κ_4 and η. These parameters are determined by fitting the model predictions to the swine-carotid-artery smooth-muscle tissue isometric tensile test active-stress vs. time data obtained by Dillon et al. (1981) and Dillon and Murphy (1982). In this type of test, the length of the pre-stretched specimen (still under tension) is kept constant while extracellular [Ca^{2+}] is (abruptly) increased. This causes temporal evolution of (and ultimate attainment of a steady-state value for) smooth-muscle tissue contraction and the associated tensile stress (within the active branch of the mechanical model). It should be noted that in accordance with Eq. (13), temporal evolution of the active stress is affected both by the instantaneous values of the chemical variables n_1–n_4 and by the instantaneous value of the mechanical variable λ_{fc}. By proper time integration of Eq. (1), and using the rate constant values listed above, temporal evolution of n_1–n_4 can be readily determined. As far as the temporal evolution of λ_{fc} is concerned, in accordance with Eq. (10), it requires the knowledge of the parameters η and κ_3. Furthermore, in accordance with Eq. (14), determination of the active-stress steady-state value entails the knowledge of the parameter λ_f. It should be noted that the parameter κ_4 only indirectly, via Eqs. (11)–(13), affects the temporal evolution of λ_{fc} and the active stress during isometric tensile testing. Consequently, this parameter was determined using the concept of the maximum load-bearing capacity of the contractile apparatus. This capacity is defined as the maximum stress that the contractile apparatus can support, during an abrupt increase in the specimen length. Application of a still larger elongation to the specimen causes mechanical failure of the contractile apparatus (i.e. detachment of all myosin heads from

the actin filaments and a complete loss of the load-carrying capacity). The value of κ_4 is found by matching the model predictions to the experimental data pertaining to the maximum load-bearing capacity data as obtained in the work of Dillon and Murphy (1982). As mentioned above, to obtain the values of the four parameters within the active portion of the smooth-muscle-tissue mechanical model, the model predictions pertaining to the temporal evolution of the first Piola-Kirchhoff stress during the activation portion of the isometric tensile test, and pertaining to the maximum load-carrying capacity obtained in the aforementioned test associated with an abrupt sample stretch, are matched with their experimental counterparts of Dillon et al. (1981) and Dillon and Murphy (1982) for isometric testing of swine-carotid-artery smooth-muscle tissue. This parameter-identification procedure yielded: (a) $\mu_f = 1.91$ MPa ; (b) $\kappa_3 = 1.91$ MPa ; (c) $\kappa_4 = 0.32$ MPa ; and (d) η = 38.2 MPa.s.

Parameterization of the Passive Part of the Model

As mentioned earlier, the passive part of the smooth-muscle-tissue mechanical model is characterized by six parameters: K, μ_ε, β, α_2, α_3, and τ. These parameters were determined by fitting model predictions to the stretch-rate vs. time data from the isotonic tensile tests conducted by Dillon et al. (1981) and Dillon and Murphy (1982) on smooth-muscle-tissue from swine carotid artery. In this type of test, the specimen is first subjected to an isometric test and then the longitudinal stress is abruptly decreased (and kept constant afterwards). Since the passive part of the mechanical model contains elastic elements, the abrupt decrease in the stress is associated with an abrupt decrease in the corresponding stretch (the so-called "*elastic recoil*"). However, since the passive part of the model also includes viscous behavior, the stretch continues to evolve with time towards its final (steady-state) value. It is the initial abrupt decrease in the stretch, the rate of subsequent stretch decrease and the stretch steady-state value that are used to determine the aforementioned six parameters (via a multiple regression curve-fitting procedure). It should be noted that within this fitting procedure, the passive portion of the smooth-muscle cell tissue is assumed to be nearly incompressible, and, hence, K is set to a large value (= 10 μ_ε). The parameter-identification procedure described above yielded the following values for the six parameters of the passive part of the material mechanical model: (a) K = 630 kPa; (b) μ_ε = 63 kPa; (c) $\beta = 0.14$; (d) $\alpha_2 = 0$; (e) $\alpha_3 = 10$; and (f) $\tau = 0.50$ s.

Model Validation and Application

The model presented in the previous section is used in this section to reveal the basic response of the swine-carotid-artery smooth-muscle tissue during isometric and isotonic tensile testing. In addition, model predictions are compared with experimental results obtained in the work of Dillon et al. (1981) and Dillon and Murphy (1982). It should be noted that all the calculations carried out in this portion of the work involved MATLAB (2012), a general-purpose mathematical package.

Isometric Tensile Test

The isometric tensile test is conducted using the following steps: (a) the test specimen is first stretched to the so-called "*optimal length*" of the smooth-muscle-tissue (corresponding to $\lambda_3 = 1.6$, in the case of swine-carotid-artery smooth-muscle tissue (Kamm et al., 1989)); (b) the pre-stretched specimen is allowed to fully relax while, due to a low [Ca^{2+}], the contractile apparatus is assumed to be inactive. These conditions result in: $n_1 = 1.0, n_2 = n_3 = n_4 = 0.0$, $\lambda_{fc} = \lambda_3$ and $\lambda_v = \lambda_3 / J^{1/3}$; (c) the specimen length is then fixed throughout the remainder of the test, while extracellular [Ca^{2+}] is abruptly increased to a value of 1.6 mM, Figure 6(a). The [Ca^{2+}] increase promotes the bonding of the myosin heads to the actin filaments and gives rise to the contraction of the contractile apparatus. This in turn causes the development of an "*active stress*"; and (d) the temporal evolution of the (longitudinal component of the) first Piola-Kirchhoff stress is then monitored. It should be noted that the longitudinal component of the first Piola-Kirchhoff stress is numerically equal to the ratio of the corresponding force (in the deformed configuration) and the specimen cross-sectional area (in the reference configuration).

Temporal evolution of the four chemical state variables following an abrupt increase in the extracellular [Ca^{2+}] is depicted in Figure 6(b). Examination of the results shown in this figure reveals that: (a) it takes about 100 s for the chemical-state variables to attain the (new) steady-state values; and (b) in the new steady-state, most of the cross-bridges are in the s_4 (latch) state in which they contribute to the (active) force transmission.

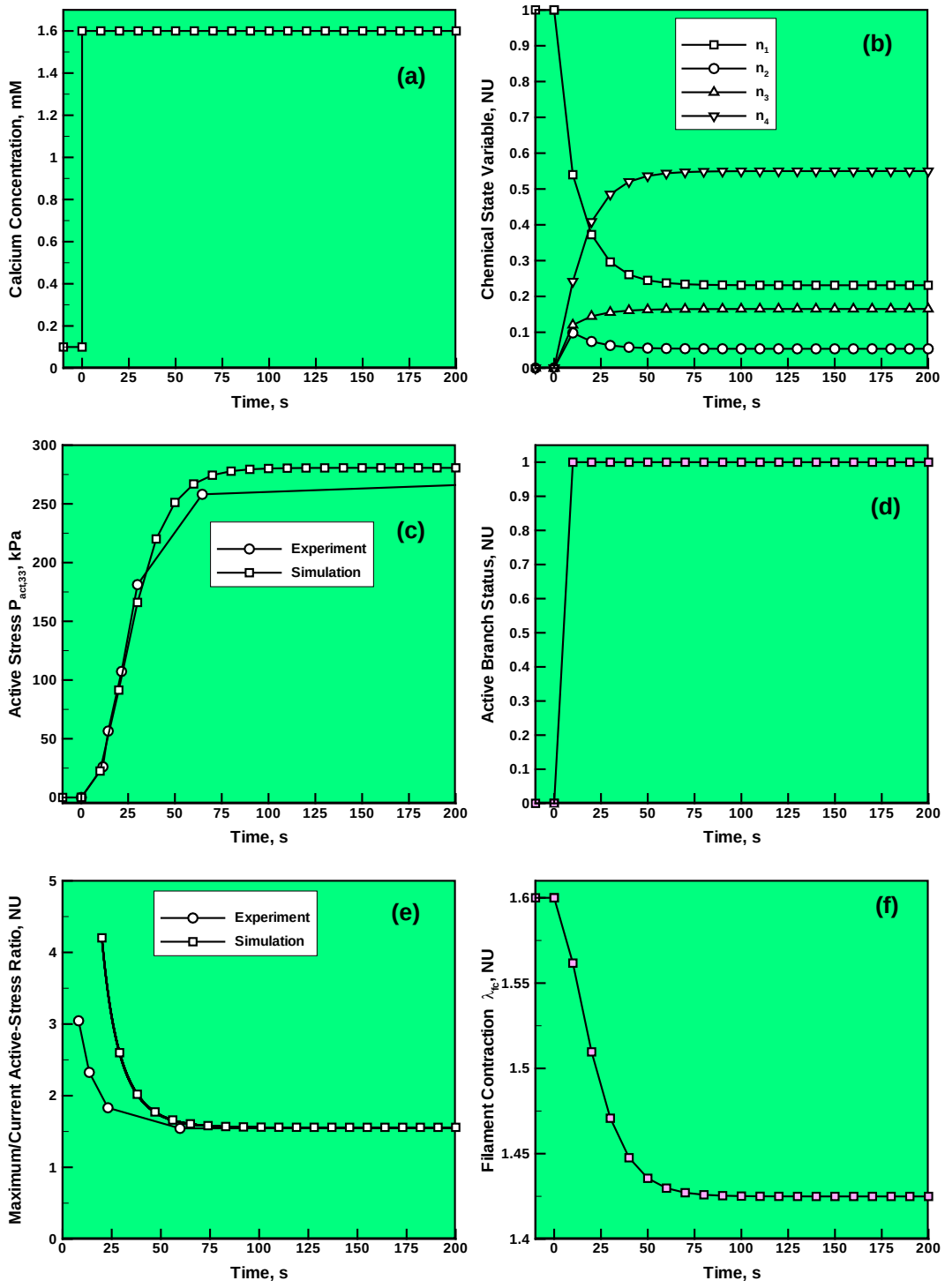

FIGURE 6 EXAMPLES OF THE TYPICAL RESULTS OBTAINED IN THE ISOMETRIC UNIAXIAL TENSILE TEST ON SWINE-CAROTID-ARTERY SMOOTH-MUSCLE TISSUE, INVOLVING PRE-STRETCH AND A SUBSEQUENT INCREASE IN THE EXTRA-CELLULAR [Ca^{2+}] FROM 0.1 mM TO 1.6 mM. THE RESULTS SHOW TEMPORAL EVOLUTION OF: (a) [Ca^{2+}]; (b) FOUR CHEMICAL-STATE VARIABLES; (c) ACTIVE FIRST PIOLA-KIRCHHOFF STRESS; (d) ACTIVE-BRANCH STATUS; (e) MAXIMUM-TO-CURRENT ACTIVE-STRESS RATIO; AND (f) FILAMENT CONTRACTION

Temporal evolution of the longitudinal component of the first Piola-Kirchhoff active stress, as predicted by the model, is depicted in Figure 6(c). Also shown in Figure 6(c) are the experimental results obtained by Dillon and Murphy (1982). Examination of the results displayed in Figure 6(c) reveals that: (a) the active stress also attains its steady-state value after approximately 100 s. This finding should be expected since the increase in the active stress depends on the increase of the four chemical-state variables, $n_1 - n_4$ (as well as on the evolution of the mechanical state variable, λ_{fc}); and (b) the agreement between the

model predictions and the experimental data is reasonably good.

Temporal evolution of the kinematic state of the filament within the active branch, as predicted by the model, is depicted in Figure 6(d). Examination of this figure shows that the contractile apparatus resides, during the present isometric tensile test, within the contracting state of the filament. Within this state, the magnitude of the active stress exceeds the elastic resistance, which results in filament contraction, i.e. $\dot{\lambda}_{fc} < 0$. Furthermore, the structural integrity of the contractile unit is never compromised.

Temporal evolution of the ratio of the maximum load-bearing capacity of the contractile apparatus and the current active stress, as predicted by the model, is depicted in Figure 6(e). Also shown in Figure 6(e) are the experimental results obtained by Dillon and Murphy (1982). Examination of the two sets of results shows that, with the exception of the short-term behavior, the agreement is fairly good. It should be noted that for the isometric tensile test, the following relationship holds:

$$\partial \psi_{\text{act}} / \partial \lambda_{fc} = -\left(\lambda_3 / \lambda_{fc}\right) \partial \psi_{\text{act}} / \partial \lambda_3 = -\left(\lambda_3 / \lambda_{fc}\right) P_{\text{act},33}.$$

Consequently, the maximum load-carrying capacity previously defined by the condition

$$-\partial \psi_{\text{act}} / \partial \lambda_{fc} = \kappa_3 n_3 + \kappa_4 n_4$$

can be defined as $P_{\text{act,max}} = \left(\lambda_{fc} / \lambda_3\right)\left(\kappa_3 n_3 + \kappa_4 n_4\right)$.

Temporal evolution of the fiber-contraction stretch ratio λ_{fc}, as predicted by the model, is depicted in Figure 6(f). Examination of the results shown in this figure reveals that it takes about 100 s for this mechanical quantity to attain its new steady-state value. This finding is expected since the four chemical-state variables, active stress and λ_{fc} are mutually related, and so are their histories.

Isotonic Tensile Test

The isotonic test follows the isometric test and includes an abrupt reduction in the longitudinal component of the first Piola-Kirchhoff total stress (from its value at the end of the isometric test). This component of the stress is subsequently held constant over the duration of the test. In the present case, the longitudinal component of the first Piola-Kirchhoff stress is reduced from its initial value of 353.2 kPa to a value of 260 kPa, Figure 7(a).

The temporal evolution of λ_3 and λ_v, as predicted by the model for the aforementioned abrupt reduction in the longitudinal component of the first Piola-Kirchhoff stress, is depicted in Figure 7(b). Examination of the results depicted in this figure shows that: (a) λ_3 drops instantaneously (the elastic recoil effect) from the initial value of 1.6 to ca. 1.551; (b) λ_3 continues to decrease but at a very low rate; and (c) due to its viscous nature, λ_v decreases asymptotically towards its zero-stress steady-state value. It should be noted that the relaxation rate of λ_v decreases with an increase in τ and with a decrease in $\beta\mu_\varepsilon$.

The effect of the longitudinal component of the first Piola-Kirchhoff stress level, which is being kept constant during the isotonic tensile test, on the initial stretch rate of the specimen (following the elastic recoil) $\dot{\lambda}_0$, as predicted by the model, is depicted in Figure 7(c). Also shown in Figure 7(c) are the experimental results obtained by Dillon et al. (1981). It should be noted that the experimental results of Dillon et al. (1981) are used to parameterize the model. Hence, the level of agreement observed in Figure 7(c) is a measure of the overall quality of the model and the success of its parameterization.

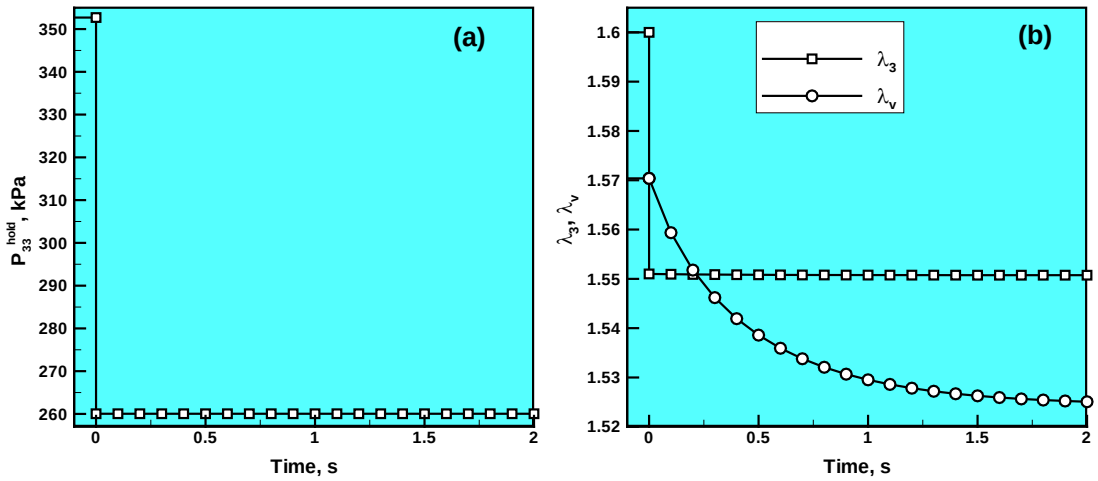

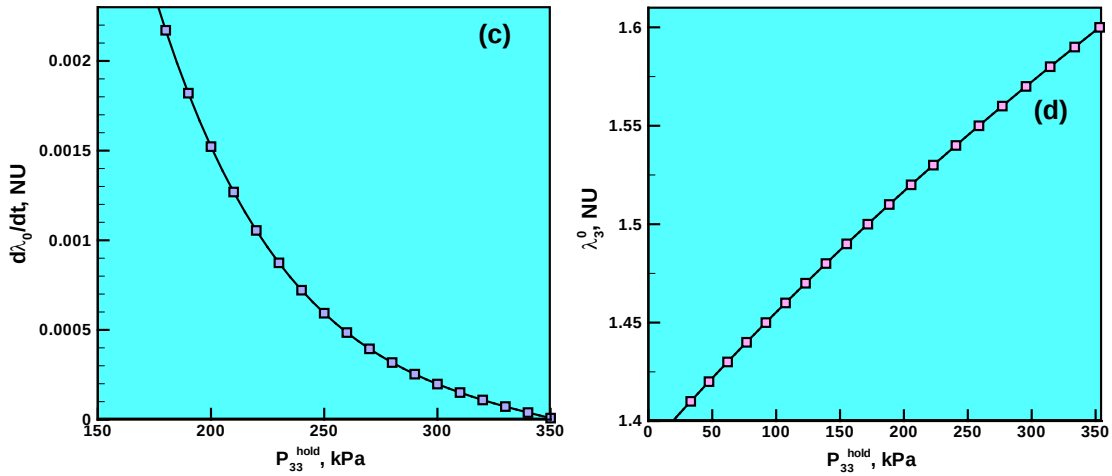

FIGURE 7. EXAMPLES OF THE TYPICAL RESULTS OBTAINED IN THE ISOTONIC UNIAXIAL-TENSILE-TEST ON SWINE-CAROTID-ARTERY SMOOTH-MUSCLE TISSUE, INVOLVING PRE-STRETCH $\lambda_3 = 1.6$, FOLLOWED BY AN INCREASE IN THE EXTRA-CELLULAR [Ca^{2+}] FROM 0.1 mM TO 1.6 mM, AND CONCLUDED BY A REDUCTION IN THE LONGITUDINAL TENSILE/HOLDING STRESS. THE RESULTS SHOW TEMPORAL EVOLUTION OF: (a) THE FIRST PIOLA-KIRCHHOFF P_{33}^{hold} STRESS; (b) TEMPORAL EVOLUTION OF TOTAL, λ_3, AND VISCOUS, λ_v, LONGITUDINAL STRETCHES; AND THE EFFECT OF THE HOLDING STRESS ON: (c) INITIAL REDUCTION-RATE OF λ_3; AND (d) INSTANTANEOUS VALUE OF λ_3 FOLLOWING ELASTIC RECOIL

The results depicted in Figures 7(a)–(c) all correspond to the case of the longitudinal component of the first Piola-Kirchhoff stress level being reduced from 353.2 kPa to 260 kPa. Several other isotonic tests are simulated within which the stress was reduced from its initial value to different levels. An example of the results obtained in these simulations is depicted in Figure 7(d). In this figure, the effect of the longitudinal component of the first Piola-Kirchhoff isotonic-test-stress on the value of λ_3 obtained after elastic recoil is shown. The results displayed in this figure show that, as expected, when the stress is kept at its initial value, no elastic recoil takes place (λ_3 remains equal to 1.6). On the other hand, as the isotonic stress level decreases, the instantaneous drop in λ_3 increases (i.e. the extent of elastic recoil increases).

Finite-Element Implementation/Usage of the Model

Finite-Element Implementation

The material model presented, parameterized and applied (to the isometric and isotonic uniaxial-tensile-loading test cases) in the previous section is implemented, in the present section, into a VUMAT user material subroutine and linked with the commercial finite-element code ABAQUS/Explicit (2011). The task of the user subroutine is to use the deformation gradient, current mass density and values of the state variables (from the previous time step) in order to update the (Cauchy) stress state and the material variables at the given material point in the current configuration. In the case of the present model, the following quantities are defined as state variables: n_1, n_2, n_3, n_4, $\mathbf{C}_v$ and λ_{fc}.

To calculate/update the stress state and the state variables within the new time-step the following iterative procedure is used:

(a) Eq. (1) is integrated in order to update the four chemical-state variables n_1–n_4;

(b) The deformation gradients of the three branches are set equal to the value of $\mathbf{F}$ that is provided to the user material subroutine by the ABAQUS/Explicit solver;

(c) Next, the corresponding Jacobian, isochoric part of $\mathbf{F}$ (Eq. (15)) and Cauchy-Green deformation tensor (Eq. (4)) are calculated;

(d) Since the third branch is purely elastic and, hence, its response is time-invariant and dependent on $\mathbf{C}$, the volumetric (Eq. (24)) and steady-state (Eq. (25)) components of the stress associated with this branch are calculated;

(e) Evolution equation for λ_{fc} (Eq. (10)) is then integrated over the duration of a given time step in order to update this quantity;

(f) The updated λ_{fc} is then used to obtain the active part of the stress, i.e. the stress associated with the first/active branch (Eq. (14));

(e) The evolution equation for the viscous component of the stress (Eq. (28)) is combined with the following

approximate expression for the time-derivative of $\mathbf{S}_v$

$$\left.\frac{d\mathbf{S_v}}{dt}\right|_{\mathbf{C}=\text{const}} \approx \frac{\mathbf{S_v}\left(\mathbf{C}_{i+1}, \mathbf{C}_{v,i+1}\right) - \mathbf{S_v}\left(\mathbf{C}_{i+1}, \mathbf{C}_{v,i}\right)}{\Delta t} \quad (31)$$

where subscripts $\mathbf{C}_{i+1}$, $\mathbf{C}_{v,i+1}$ and $\mathbf{C}_{v,i}$ are used to denote the values of $\mathbf{S}_v$ computed via Eq. (26) for $\mathbf{C}$ and $\mathbf{C}_v$ evaluated at either the current (i+1) or the previous (i) time increments. The resulting equation is solved for the unknown $\mathbf{S_v}\left(\mathbf{C}_{i+1}, \mathbf{C}_{v,i+1}\right)$; and

(f) Lastly, the updated value of the viscous stress is used to obtain the corresponding updated value of $\mathbf{C}_v$, i.e. $\mathbf{C}_{v,i+1}$ via Eq. (26). It should be noted that Eq. (26) represents a system of six linear algebraic equations with six unknowns.

Implementation Validation

The model implemented into the user-material subroutine is then validated by re-simulating the isometric and isotonic uniaxial tensile tests previously described in Section VII. The results obtained are identical to their counterparts reported in Figures 6(a)–(f) and 7(a)–(d), confirming the validity of the model implementation.

Application of the Model to a Simple Contraction Problem

1) Problem Formulation

In this section, the user-material subroutine described and validated in the previous two sections is utilized in the context of a simple smooth-muscle contraction problem in order to demonstrate its utility. The problem analyzed involves a tubular structure made of smooth muscles with the cells' longitudinal direction aligned with the circumferential direction of the structure. In addition, tube intra-luminal content is modeled as a prolate spheroidal with the major/unique axis collinear with the tube axis. The minor axis of the spheroidal, on the other hand, is made slightly larger than the inner radius of the tube (i.e. the spheroidal and the tube are initially in contact over a small area). The contact stresses activate smooth muscles, in the contact region, by increasing the cytosolic [Ca^{2+}]. This, in turn, causes longitudinal contraction of the activated ("*awakened*") smooth-muscle cells, which gives rise to the local circumferential/radial contraction of the tube. The contraction of the tubular structure then increases the ellipsoidal/tube contact stresses and, hence, the net force acting on the ellipsoidal in the tube-axis direction. This results in the forward displacement of the ellipsoidal. As a result of the downward displacement of the ellipsoidal, a new spheroidal/tube contact region is generated and a new tubular section of the smooth muscle is activated. This, in turn, results in further forward advancement of the ellipsoidal, and the whole sequence of processes described above repeats.

2) Geometrical Model

The initial geometry of the computational domain, consisting of the previously described tubular and ellipsoidal structures, is depicted in Figure 8(a). The initial dimensions of the two structures are as follows: (a) tube – length = 30 mm; outer radius = 5 mm; inner radius = 3 mm; and (b) ellipsoid – major axis = 6 mm; minor axis = 3.025 mm. The longitudinal axes of the tube/ellipsoidal are aligned in the z-direction.

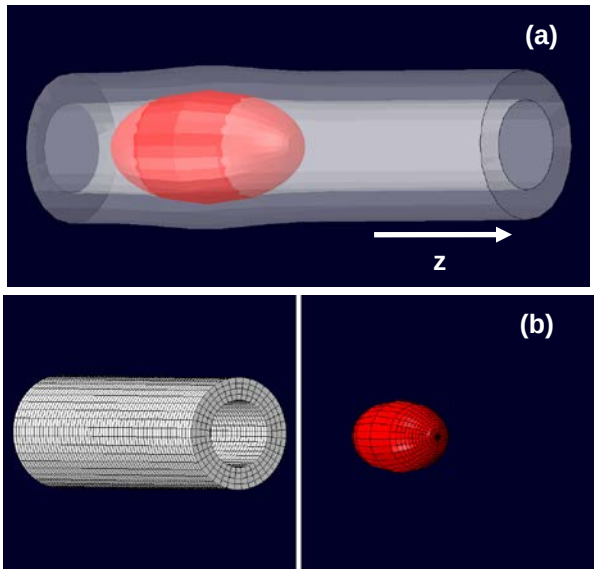

FIGURE 8. TYPICAL: (a) GEOMETRICAL; AND (b) MESHED MODELS OF THE TUBE AND ELLIPSOIDAL USED IN THE SIMULATIONS OF SMOOTH-MUSCLE CONTRACTION

3) Meshed Model

The geometrical model described above is meshed in the following way: (a) the tube is meshed using 4, 40 and 60 elements in the through-the-thickness, circumferential and longitudinal directions, respectively. The elements used are eight-node, hexahedral, first-order, continuum elements; and (b) the ellipsoid is meshed using 616 quadrilateral and 56 triangular membrane elements. For simplicity, the ellipsoidal is treated as a rigid body with six (three translational and three rotational) degrees of freedom. Typical finite-element meshes used in the present work for the two parts of the computational domain are displayed in Figure 8(b). All meshing carried out in the present work was done using HyperMesh (2012), a general-purpose

pre-processing software from Altair Engineering, Inc.

4) Material Model

The tubular structure is assigned the smooth-muscle material model overviewed, parameterized and validated in the previous sections. As far as the spheroidal-shaped intra-luminal content is concerned, it is treated as a rigid body and, hence, no material model formulation (except for the mass density) had to be specified.

5) Initial Conditions

The tubular structure, in its original configuration, is assumed to be in equilibrium with the interacting ellipsoidal and to contain stresses developed within the passive portion of the material as a result of the tube/ellipsoidal contact stresses. Both the tube and the ellipsoidal are initially assumed to be quiescent.

6) Boundary Conditions

Fixed-displacement boundary conditions are applied in the longitudinal direction of the tube, to one of the tube ends. In addition, zero-stress conditions are applied to all the free surfaces of the tube and the ellipsoidal.

7) Contact Interactions

The tube-ellipsoidal normal interactions are analyzed using a penalty-contact algorithm. Within this algorithm, (normal) penetration of the contacting surfaces is resisted by a set of linear springs which produce a contact pressure that is proportional to the depth of tube/ellipsoidal penetration. To minimize penetration, the maximum values, which still ensure computational stability, are assigned to the (penalty) spring constants. Force equilibrium in a direction collinear with the contact-interface normal then causes the penetration to acquire an equilibrium (contact-pressure-dependent) value. It should be noted that no contact pressures are developed unless (and until) the nodes on the (ellipsoidal) "*slave surfaces*" contact/penetrate the (tube inner) "*master surfaces*". On the other hand, the magnitude of the contact pressure that can be developed is unlimited. As far as the tangential tube-ellipsoidal interactions (responsible for transmission of the shear stresses across the contact interface) are concerned, they are modeled using the Coulomb friction law. Within this law, the maximum value of the shear stresses that can be transmitted (before the contacting surfaces begin to slide) is defined by a product of the contact pressure and a static (before sliding) and a kinetic (during sliding) friction coefficient.

8) Computational Procedure

Explicit, transient, non-linear-dynamics finite element analyses are employed while ensuring that the stability criterion is met through the proper and adaptive selection of the time increment. As mentioned earlier, all the calculations carried out in the present work were performed using ABAQUS/ Explicit (2011).

9) Computational Accuracy, Stability and Cost

A standard mesh sensitivity analysis was carried out (the results not shown for brevity) in order to ensure that the results obtained are accurate, i.e. insensitive to further reductions in the size of the elements used. A typical 10-second computational analysis followed by a detailed post-processing data reduction analysis required on average 30 minutes of (wall-clock) time on a 12-core, 3.0 GHz machine with 16 GB of memory.

10) Typical Results

An example of the typical results is depicted in Figures 9(a)–(d). The results depicted in these figures show the spatial distribution of the two materials/bodies, i.e. of the smooth-muscle tissue in the form of a tubular section, and the ellipsoidal-shaped intra-luminal content at four times (2 sec, 4 sec, 6 sec, and 8 sec) measured from the instant of initial activation of the muscle. Examination of the results shown in Figures 9(a)–(d) clearly reveals that: (a) the contact stresses at the tube/ellipsoidal interfaces promote smooth-muscle tissue contraction; (b) as a result of this contraction, forward momentum is imparted to the ellipsoidal, giving rise to its advancement along the tube axis; and (c) once the ellipsoidal has advanced and the contracted smooth-muscle tissue no longer experiences contact pressure, the tissue relaxes and the tube acquires its original cross-section.

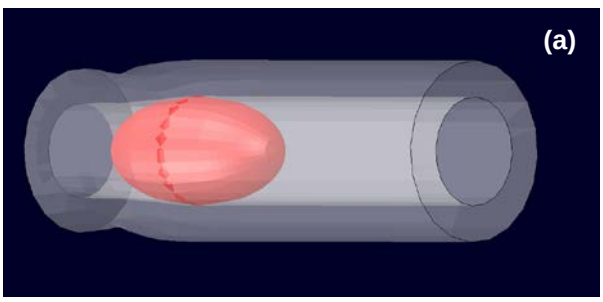

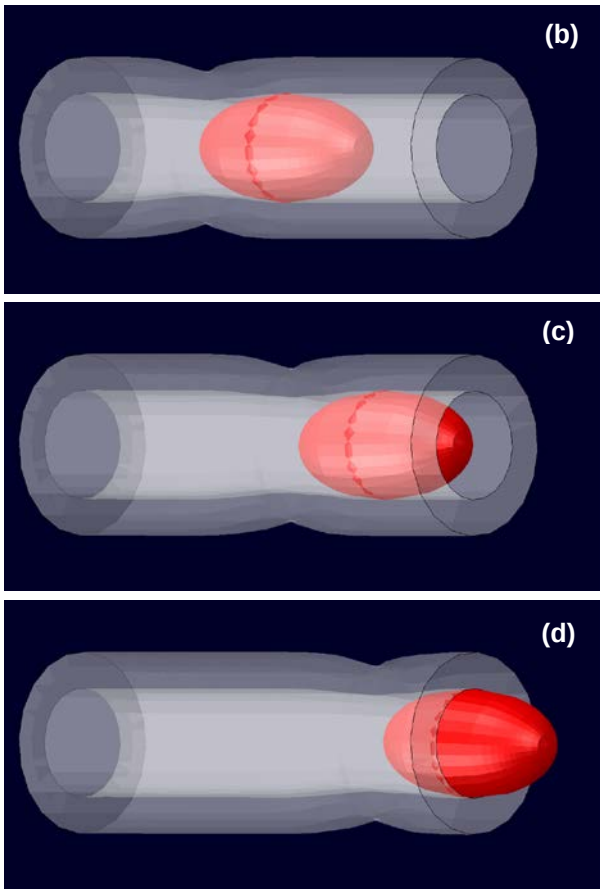

FIGURE 9. SPATIAL DISTRIBUTION OF THE SMOOTH-MUSCLE TISSUE IN THE FORM OF A TUBULAR SECTION, AND THE ELLIPSOIDAL-SHAPED INTRA-LUMINAL CONTENT, AT FOUR TIMES MEASURED FROM THE INSTANT OF INITIAL ACTIVATION OF THE MUSCLE: (a) 2 sec; (b) 4 sec; (c) 6 sec; AND (d) 8 sec

Temporal evolution of the axial position of the ellipsoidal center of mass is shown in Figure 10(a). It is seen that the motion of the ellipsoidal is not smooth but rather jerky. That is, occasionally the ellipsoidal "*runs away*" from the contracting smooth-muscle tissue and comes to rest. Then, the contact stresses activate the tissue in the region surrounding the contact interface, causing additional advancement of the ellipsoidal. Temporal evolution of the radial displacement at one of the points which is located at the interior surface of the tube, and halfway along its length, is depicted in Figure 10(b). It is seen that as expected: (a) the smooth-muscle tissue is initially in the relaxed state, which is characterized by zero radial displacement at the location described above; (b) as the ellipsoidal begins to approach the target point, the radial displacement first begins to acquire positive values (i.e. the tube begins to expand in the radial direction in order to accommodate the slightly-oversized ellipsoidal); (c) as the tube/ellipsoidal contact interface passes through the target point, the radial displacement begins to decrease and ultimately acquires negative values (as a result of the smooth-muscle tissue contraction); and (d) once the ellipsoidal has advanced sufficiently far from the target point, the muscle-tissue begins to relax, causing the radial displacement to start approaching its initial (zero) value.

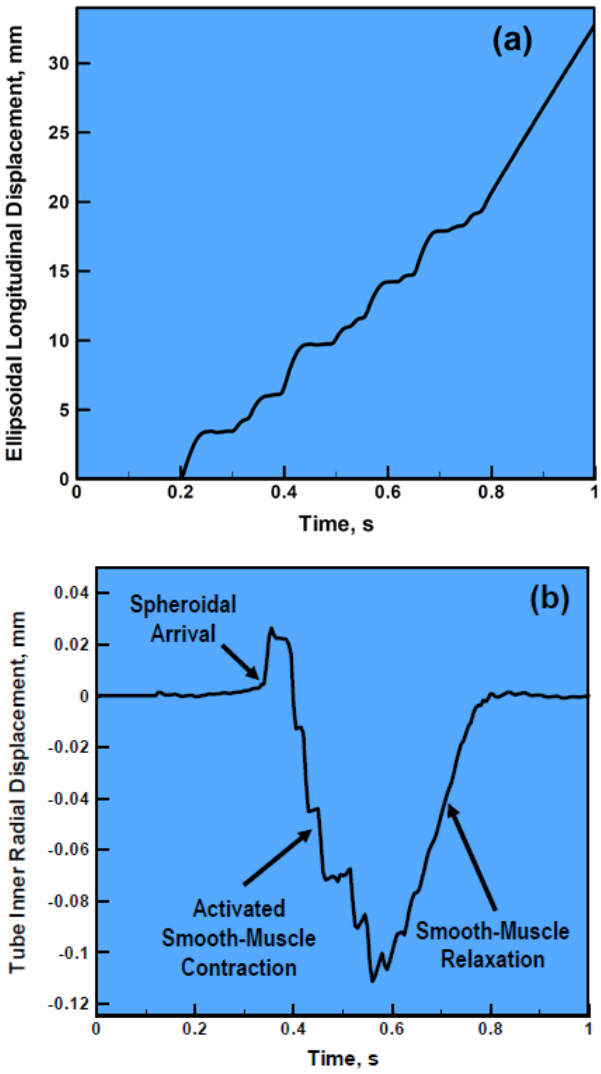

FIGURE 10. (a) TEMPORAL EVOLUTION OF THE AXIAL POSITION OF THE ELLIPSOIDAL CENTER OF MASS; AND (b) TEMPORAL EVOLUTION OF THE RADIAL DISPLACEMENT AT ONE OF THE POINTS WHICH IS LOCATED AT THE INTERIOR SURFACE OF THE TUBE, AND HALFWAY ALONG ITS LENGTH

Summary and Conclusions

Based on the results obtained in the present work, the following summary remarks and main conclusions can be drawn:

1. A critical assessment, parameterization (using experimental data, for isometric (constant length) and isotonic (constant holding stress) uniaxial-tensile-tests of swine carotid artery,

obtained by Dillon et al. (1981) and Dillon and Murphy (1982)) and validation of the smooth-muscle-tissue material model originally proposed by Kroon (2010) has been conducted. It has been shown that, for the most part, the model correctly accounts for key aspects of the smooth-muscle-tissue behavior under these loading conditions.

2. The model is next implemented into a user-material subroutine within which, for a given incremental deformation, the stress state as well as the values of the material-state variables are updated over a small time step.
3. The user-material subroutine is then linked with a commercial finite-element program and used to carry out a computational analysis of a simple smooth-muscle contraction problem involving: (a) a tubular structure surrounded with smooth-muscle tissue (with muscle-cell longitudinal directions aligned in the tube circumferential direction); and (b) an intra-luminal content in the form of a prolate spheroidal with the spheroidal major axis coinciding with the tube axis.

The results of the computational investigation have clearly demonstrated how activation/contraction of the smooth-muscle tissue triggered by the tube/spheroidal contact stresses results in a forward momentum/ motion of the intra-luminal content.

ACKNOWLEDGMENTS

A. G. would like to acknowledge the guidance and support of Professor Delphine Dean of the Department of Bioengineering at Clemson University.

REFERENCES

Altair Engineering, Inc., HyperMesh 12.0, 2012.

Arner, A. "Mechanical characteristics of chemically skinned guinea-pig taenia coli." Pflügers Archiv –European Journal of Physiology 395 (1982): 277–284.

Bitar, K. N. "Function of gastrointestinal smooth muscle: from signaling to contractile proteins." American Journal of Medicine 115 (2003): 15S–23S.

Brophy, C. M. "The dynamic regulation of blood vessel caliber." Journal of Vascular Surgery 31 (2000): 391–395.

Chu, J.-W. and G. A. Voth. "Allostery of actin filaments: Molecular dynamics simulations and coarse-grained analysis." Proceedings of the National Academy of Sciences USA 102 (2005): 13111–13116.

Chu, J.-W. and G. A. Voth. "Coarse-grained modeling of the actin filament derived from atomistic-scale simulations." Biophysical Journal 90 (2006): 1572–1582.

Clark, J. F. and G. Pyne-Geithman. "Vascular smooth muscle function: the physiology and pathology of vasoconstriction." Pathophysiology 12 (2005): 35–45.

Dassault Systems, "ABAQUS Version 6.10EF, User Documentation", 2011.

Dillon, P. F., M. O. Aksoy, S. P. Driska, and R. A. Murphy. "Myosin phosphorylation and the crossbridge cycle in arterial smooth muscle." Science 211 (1981): 495–497.

Dillon, P. F., and R. A. Murphy. "High force development and crossbridge attachment in smooth muscle from swine carotid arteries." Circulation Research 50 (1982): 799–804.

Fay, F. S., and C. M. Delise. "Contraction of isolated smooth muscle cells—structural changes." Proceedings of the National Academy of Sciences USA 70 (1973): 641–645.

Fung, Y. C. "Mathematical representation of the mechanical properties of the heart muscle." Journal of Biomechanics 3 (1970): 381–404.

Gestrelius, S., and P. Borgström. "A dynamic model of smooth muscle contraction." Biophysical Journal 50 (1986): 157–169.

Grujicic, M., G. Arakere, P. Pisu, B. Ayalew, N. Seyr and M. Erdmann. "Application of Topology, Size and Shape Optimization Methods in Polymer Metal Hybrid Structural Lightweight Engineering." Multidiscipline Modeling in Materials and Structures 4 (2008a): 305–330.

Grujicic, M., V. Sellappan, L. Mears, X. Xuan, N. Seyr, M. Erdmann, and J. Holzleitner. "Selection of the Spraying Technologies for Over-Coating of Metal-Stampings with Thermo-Plastics for Use In Direct-Adhesion Polymer Metal Hybrid Load-Bearing Component." Materials Processing Technology 198 (2008b): 300–312.

Grujicic, M., V. Sellappan, T. He, N. Seyr, A. Obieglo, M. Erdmann, and J. Holzleitner. "Total Life-Cycle Based Materials Selection for Polymer Metal Hybrid Body-In-White Automotive Components." Journal of Materials Engineering and Performance 18 (2009a): 111–128.

Grujicic, M., V. Sellappan, G. Arakere, N. Seyr, A. Obieglo, M. Erdmann, and J. Holzleitner. "The Potential of a

Clinch-Lock Polymer Metal Hybrid Technology for Use in Load-Bearing Automotive Components." Journal of Materials Engineering and Performance 18 (2009b): 893–902.

Grujicic, M., B. P. d'Entremont, B. Pandurangan, A. Grujicic, M. LaBerge, J. Runt, J. Tarter, and G. Dillon. "A Study of the Blast-induced Brain White-Matter Damage and the Associated Diffuse Axonal Injury." Multidiscipline Modeling in Materials and Structures, 8 (2012): 213–245.

Hai, C. M., and R. A. Murphy. "Cross-bridge phosphorylation and regulation of latch state in smooth muscle." American Journal of Physiology 254 (1988): C99–C106.

Hai, C. M., and R. A. Murphy. "Cross-bridge dephosphorylation and relaxation of vascular smooth muscle." American Journal of Physiology, 256 (1989): C282–C287.

Herrera, A. M., B. E. McParland, A. Bienkowska, R. Tait, and P. D. Par. "'Sarcomeres' of smooth muscle: functional characteristics and ultrastructural evidence." Journal of Cell Science 118 (2005): 2381–2392.

Hodgkinson, J. L., T. M. Newman, S. B. Marston, and N. J. Severs. "The structure of the contractile apparatus in ultrarapidly frozen smooth muscle: freeze-fracture, deep-etch, and freeze-substitution studies." Journal of Structural Biology 114 (1995): 93–104.

Huxley, A. F. "Muscle structure and theories of contraction." Progress in Biophysics and Biophysical Chemistry 7 (1957): 255–318.

Huxley, A. F. and R. Niedergerke. "Interference microscopy of living muscle fibres." Nature 173 (1954): 971–973.

Huxley, H. E. "Electron microscope studies on the organisation of the filaments in striated muscle." Biochemica et Biophysica Acta 12 (1953): 387–394.

Huxley, H. E. and J. Hanson. "Changes in the cross-striations of muscle during contraction and stretch and their structural interpretation." Nature 173 (1954): 973–976.

Jaggar, J. H., V. A. Porter, W. J. Lederer, and M. T. Nelson. "Calcium sparks in smooth muscle." American Journal of Physiology — Cell Physiology 278 (2000): C235–C256.

Jiang, M. J., and K. G. Morgan. "Agonist-specific myosin phosphorylation and intracellular calcium during isometric contractions of arterial smooth muscle." Pflügers Archiv — European Journal of Physiology 413 (1989): 637–643.

Kamm, K. E., W. T. Gerthoffer, R. A. Murphy, and D. F. Bohr. "Mechanical properties of carotid arteries from DOCA hypertensive swine." Hypertension 13 (1989): 102–109.

Kroon, M. "A constitutive model for smooth muscle including active tone and passive viscoelastic behaviour." Mathematical Medicine and Biology 27 (2010): 129–155.

Kuo, K. H., and C. Y. Seow. "Contractile filament architecture and force transmission in swine airway smooth muscle." Journal of Cell Science 117 (2004): 1503–1511.

Lee, S., and G. W. Schmid-Schönbein. "Biomechanical model for the myogenic response in the microcirculation: part I—formulation and initial testing." Journal of Biomechanical Engineering 118 (1996a): 145–151.

Lee, S., and G. W. Schmid-Schönbein. "Biomechanical model for the myogenic response in the microcirculation: part II—experimental evaluation in rat cremaster muscle." Journal of Biomechanical Engineering 118 (1996b): 152–157.

Löfgren, M., U. Malmqvist, and A. Arner. "Substrate and product dependence of force and shortening in fast and slow smooth muscle." Journal of General Physiology 117 (2001): 407–417.

Makujina, S. R., W. Abebe, S. Ali, and S. J. Mustafa. "Simultaneous measurement of intracellular calcium and tension in vascular smooth muscle: validation of the everted ring preparation." Journal of Pharmacological and Toxicological Methods 34 (1995): 157–163.

The MathWorks Inc., MATLAB, The Language of Technical Computing, Version 8.0.0.783, R2012b.

McIntyre Jr, R. C., J. Agrafojo, and A. Banerjee. "Pulmonary vascular smooth muscle contraction." Journal of Surgical Research 61 (1996): 170–174.

Miftakhov, R. N. and G. R. Abdusheva. "Numerical simulation of excitation-contraction coupling in a locus of the small bowel." Biological Cybernetics 74 (1996): 455–467.

Morgan, K. G., P. Papageorgiou, and M. J. Jiang. "Pathophysiologic role of calcium in the development of vascular smooth muscle tone." American Journal of Cardiology 64 (1989): 35F–40F.

Paul, R. J. "Smooth muscle energetics and theories of cross-bridge regulation." American Journal of Physiology 258

(1990): C369–C375.

Peterson, J. W. "Simple model of smooth muscle myosin phosphorylation and dephosphorylation as ratelimiting mechanism." Biophysical Journal 37 (1982): 453–459.

Pfaendtner, J., E. Lyman, T. D. Pollard, and G. A. Voth. "Structure and dynamics of the actin filament." Journal of Molecular Biology 396 (2010): 252–263.

Rachev, A. and K. Hayashi. "Theoretical study of the effects of vascular smooth muscle contraction on strain and stress distributions in arteries." Annals of Biomedical Engineering 27 (1999): 459–468.

Rembold, C. M. and R. A. Murphy. "Myoplasmic [Ca^{2+}] determines myosin phosphorylation and isometric stress in agonist-stimulated swine arterial smooth muscle." Journal of Cardiovascular Pharmacology 12 (1988): S38–S42.

Rembold, C. M. and R. A. Murphy. "Latch-bridge model in smooth muscle: [Ca^{2+}] can quantitatively predict stress." American Journal of Physiology 259 (1990): C251–C257.

Rosenbluth, J. "Smooth muscle: an ultrastructural basis for the dynamics of its contraction." Science 148 (1965): 1337–1339.

Roy, S., P. Silacci, and N. Stergiopulos. "Biomechanical properties of decellularized porcine common carotid arteries." American Journal of Physiology –Heart and Circulatory Physiology 289 (2005): 1567–1576.

Seow, C. Y. and P. D. Par. "Ultrastructural basis of airway smooth muscle contraction." Canadian Journal of Physiology and Pharmacology 85 (2007): 659–665.

Silver, F. H., P. B. Snowhill, and D. J. Foran. "Mechanical behavior of vessel wall: a comparative study of aorta, vena cava, and carotid artery." Annals of Biomedical Engineering 31 (2003): 793–803.

Singer, H. A. and R. A. Murphy. "Maximal rates of activation in electrically stimulated swine carotid media." Circulation Research, 60 (1987): 438–445.

Stålhand, J., A. Klarbring, and G. A. Holzapfel. "Smooth muscle contraction: mechanochemical formulation for homogeneous finite strains." Progress in Biophysics and Molecular Biology 96 (2008): 465–481.

Takamizawa, K. and K. Hayashi. "Strain energy density function and uniform strain hypothesis for arterial mechanics." Journal of Biomechanics 20 (1987): 7–17.

Tang, D. C., J. T. Stull, Y. Kubota, and K. E. Kamm. "Regulation of the [Ca^{2+}] dependence of smooth muscle contraction." Journal of Biological Chemistry 267 (1992): 11839–11845.

Tosun, M., R. J. Paul, and R. M. Rapoport. "Intracellular [Ca^{2+}] elevation and contraction due to prostaglandin F2alpha in rat aorta." European Journal of Pharmacology 340 (1997): 203–208.

Walker, J. S., C. J. Wingard, and R. A. Murphy. "Energetics of crossbridge phosphorylation and contraction in vascular smooth muscle." Hypertension 23 (1994): 1106–1112.

Yang, J., J. W. Clark Jr, , R. M. Bryan, and C. Robertson. "The myogenic response in isolated rat cerebrovascular arteries: smooth muscle cell model." Medical Engineering Physics 25 (2003a): 691–709.

Yang, J., J. W. Clark Jr, , R. M. Bryan, and C. Robertson. "The myogenic response in isolated rat cerebrovascular arteries: vessel model." Medical Engineering Physics 25 (2003b): 711–717.

Zulliger, M. A., A. Rachev, and N. Stergiopulos. "A constitutive formulation of arterial mechanics including vascular smooth muscle tone." American Journal of Physiology–Heart and Circulatory Physiology 287 (2004): H1335–H1343.